BioNanoSci. (2017) 7:546–553
DOI 10.1007/s12668-017-0420-4

Soxhlet Extraction of Neem Pigment to Synthesize Iron Oxide Nanoparticles and Its Catalytic and Adsorption Activity for Methylene Blue Removal

Priyabrata Pal[1] · **Salma S. Syed**[1] · **Fawzi Banat**[1]

Published online: 21 June 2017

Abstract Green synthesis of iron oxide nanoparticles is gaining importance recently due to its cost-effectivity and ecofriendly treatment technique. The aim of the present study is to concentrate neem (*Azadirachta indica*) leaf pigment using Soxhlet extraction and to synthesize iron oxide nanoparticles and to check its efficacy in degrading methylene blue dye in aqueous solution. Characterization of the synthesized iron oxide nanoparticles is carried out using X-ray diffraction (XRD), Fourier Transform Infrared (FTIR) spectroscopy, Scanning Electron Microscopy (SEM) equipped with Energy Dispersive X-ray (EDX) spectroscopy, Transmission Electron Microscopy (TEM), and Vibrating Sample Magnetometer (VSM) analysis. The characterization results confirm the formation of iron oxide (α-Fe_2O_3) nanoparticles. Obtained nanoparticles were evaluated for degradation and adsorption of methylene blue (MB) dye. It enhanced the degradation of methylene blue dye to 95.93% in the presence of 0.1 (N) sodium hydroxide solution (82.69% in the absence of α-Fe_2O_3). The maximum uptake capacity of MB was increased from 64.1 to 99.0 mg/g using native calcium alginate hydrogel and calcium alginate impregnated with produced iron oxide nanoparticle composite hydrogel, respectively. Thus, extraction of pigment from neem leaves and synthesized iron oxide nanoparticles showed satisfactory results.

Keywords Neem leaves · Soxhlet extraction · Nanoparticles · Iron oxide · Methylene blue

✉ Priyabrata Pal
ppriyabrata@pi.ac.ae

[1] Department of Chemical Engineering, The Petroleum Institute, P.O. Box 2533, Um Al Naar, Abu Dhabi, United Arab Emirates

1 Introduction

The current global attention towards the field of nanotechnology has become rapidly increasingly important because it offers indisputable benefits to every area of expertise, including wastewater treatment [1] and environmental remediation [2]. Nanoparticles have the potential to progress the environment through the development of new solutions to environmental problems. Metallic nanoparticles have taken immense attention due to their vast applications including bio-sensing and catalysis [3, 4]. Currently, different methods are reported for the preparation of nanoparticles which can be divided into three categories: chemical, physical, and biological methods. Physical methods are well known to produce metallic nanoparticles [5, 6]. Among them, conventional methods for making nanoparticles can generally involve either a "top down" approach or a "bottom up" approach. Synthesis of nanoparticles by "bottom up approach" includes traditional and green production methods [7]. Some of the traditional methods are co-precipitation [8], hydrothermal method [9], and hydrolysis [10]. However, methods of preparation require toxic reagents, organic solvents, or non-biodegradable agents causing the environment to be potentially dangerous.

The biosynthesis of nanoparticles has been proposed as a cost-effective, environmentally friendly alternative to chemical and physical methods. Thus, nanomaterials have been synthesized using microorganisms [11] and plant extracts [12, 13]. The ability of plant extracts to reduce metal ions has been known since early 1900s, although the rapid synthesis of bulk metallic nanoparticles was not well understood [14]. Biogenic synthesis is useful not only because of its reduced environmental impact [15] compared with some of the physicochemical production methods but also because it can be used to produce large quantities of nanoparticles that are free of contamination and have a well-defined size and morphology [16]

Biogenic synthesis of iron oxides using plant extracts has been well-known and reported using tree leaf extracts [17]. Iron oxide nanoparticles have been synthesized by using *Azadirachta indica*, also known as neem, which is a tree of mahogany family Meliaceae [18]. It is growing in tropical and semi-tropical regions and native to most Asian countries including the United Arab Emirates.

In this study, we reported the biosynthesis of iron oxide nanoparticles using neem leaves by two-step method. Neem leaves contain high amounts of different organic compounds [19]. These compounds are extracted using Soxhlet apparatus to get concentrated green pigments. Secondly, the concentrated pigments reduced ferric ions at room temperature to produce iron oxide nanoparticles. The reduction using aqueous neem leaf extracts for ferric ions is rapid and results to stable iron oxide nanoparticles. The obtained particles were identified using X-ray diffraction (XRD) and Fourier Transform Infrared (FTIR) spectroscopy analysis. The morphology and size distribution of synthesized nanoparticles were visualized by Scanning Electron Microscopy (SEM) and Transmission Electron Microscopy (TEM). Compositional analysis was performed by Energy Dispersive X-ray (EDX) analysis. The catalytic activity of the synthesized iron oxide nanoparticles was observed in the degradation of organic contaminants as methylene blue (MB) dye. Similarly, adsorption of MB dye in solutions was carried out with calcium alginate hydrogel and calcium alginate in the presence of iron oxide nanoparticles to clarify the enhancement of adsorption as well as effective composite hydrogel as adsorbent which can easily be separated from solutions using a magnet. The results suggested that iron oxide nanoparticles synthesized using neem leaf extracts are potentially useful for the removal of organic pollutants.

2 Materials and Methods

2.1 Materials

Analytical-grade ferric chloride ($FeCl_3 \cdot 6H_2O$, 98%) was purchased from Merck, Germany and used without further purification. Anhydrous ethyl alcohol (99.5% pure, 200 proof), methylene blue, and sodium hydroxide were purchased from Sigma-Aldrich, Germany. The neem (*A. indica*) leaves were collected locally from the tree in Abu Dhabi.

2.2 Instrumentation

The pictures of the extracted pigment and iron oxide nanoparticles were taken in a digital camera (Canon 60D). The crystalline structure and phase purity of the iron oxide particles were identified in X-ray diffraction (XRD) analytical X'Pert PRO powder diffractometer (Cu-Kα radiation 1.5406 Å, 40 kV, 40 mA). FTIR spectra of the iron oxide nanoparticles were recorded over the range of 500–4000 cm^{-1} on a model spectrum using Nicole Avatar 330 (FTIR) spectrophotometer. Scanning electron microscopy (SEM) was performed using a FEG Quanta 250 to study the morphology of iron oxide nanoparticles. The Energy Dispersive X-ray (EDX) spectrometry was carried out in an Oxford-EDX, UK. Transmission electron microscopy (TEM) observations were carried out on a Hitachi H-9500, Japan. The particle size distributions were determined using the ImageJ tool version 4.00 program. After the addition of neem pigment extract into aqueous solution of $FeCl_3$, UV–visible spectra were recorded over the range 300–700 nm with a UV–visible spectrophotometer (Hach Lange, DR 5000, USA). The magnetic properties of the iron oxide nanoparticles were measured at room temperature using vibrating sample magnetometer (VSM; Lakeshore Model 7404, Japan).

2.3 Preparation of Leaf Extract

The collected leaves were washed several times with deionized water to remove any impurities and kept at room temperature for natural drying. The leaves were grounded into fine powder using a mixer (Mouliex, Japan) and sieved to obtain a particle size up to 30 μm. Neem leaf powder was dried in an oven at 50 °C for 2 h and stored for further use.

2.4 Extraction of Neem Pigment

Finely powdered neem leaves of 20.0 g were kept in paper sachets and put into the Soxhlet extractor having ethyl alcohol of 200 mL. The time given for extraction of neem pigment was 10 h. Once the extraction was over, rotary evaporator was used at 45 °C for 20 min to evaporate ethyl alcohol present in the pigment. Finally, the pigment was washed with deionized water and dried in an oven at 60 °C for 2 h. The collected pigment was stored in a refrigerator for further use. The % yield of neem pigment is calculated as:

$$y = \left(\frac{\text{Mass of neem pigment extracted}}{\text{Initial mass of neem leaves}}\right) * 100 \quad (1)$$

The collected neem pigment was stored at room temperature for synthesis of iron oxide particles from ferric chloride solution.

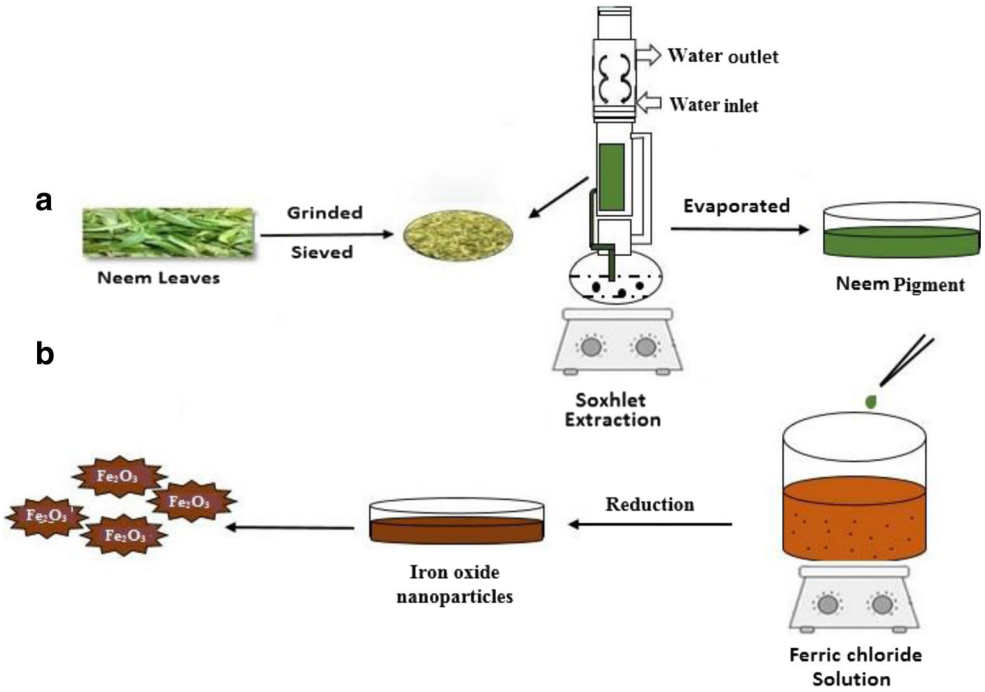

Fig. 1 Schematic diagram of (**a**) extraction of neem pigment and (**b**) synthesis of iron oxide nanoparticles

2.5 Application

2.5.1 Catalytic Degradation of Methylene Blue (MB)

Ten milliliters of methylene blue solutions having concentration of 10 mg/L was taken in conical flask. A total of 0.5 mL sodium hydroxide solution of strength 0.1 (N) were added dropwise to MB solution. Degradation of MB solution was observed in UV–vis spectrophotometer at 666 nm. Similarly, iron oxide nanoparticles were added to sodium hydroxide solution to keep the particle concentration at 1.0 wt% and added dropwise to MB solution to check the absorbance.

2.5.2 Adsorption of Methylene Blue (MB)

Sodium alginate solution (2.0 wt%) was added to 4.0 wt% calcium chloride solution to prepare calcium alginate hydrogel beads. For the preparation of iron oxide-impregnated calcium alginate composite hydrogel, 1.0 wt% iron oxide nanoparticles were added into 2.0 wt% sodium alginate solution to prepare

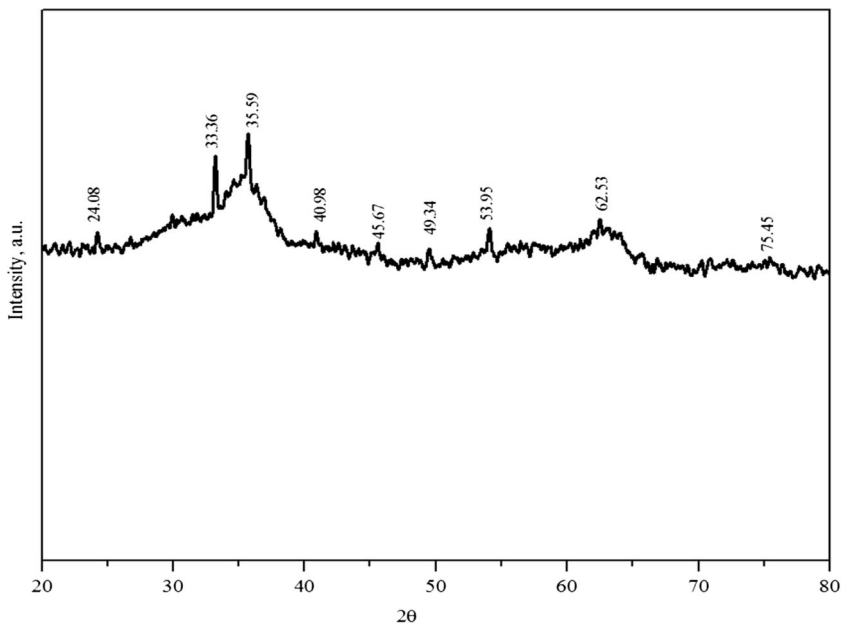

Fig. 2 XRD patterns of α-Fe_2O_3 nanoparticles extracted from neem leaves

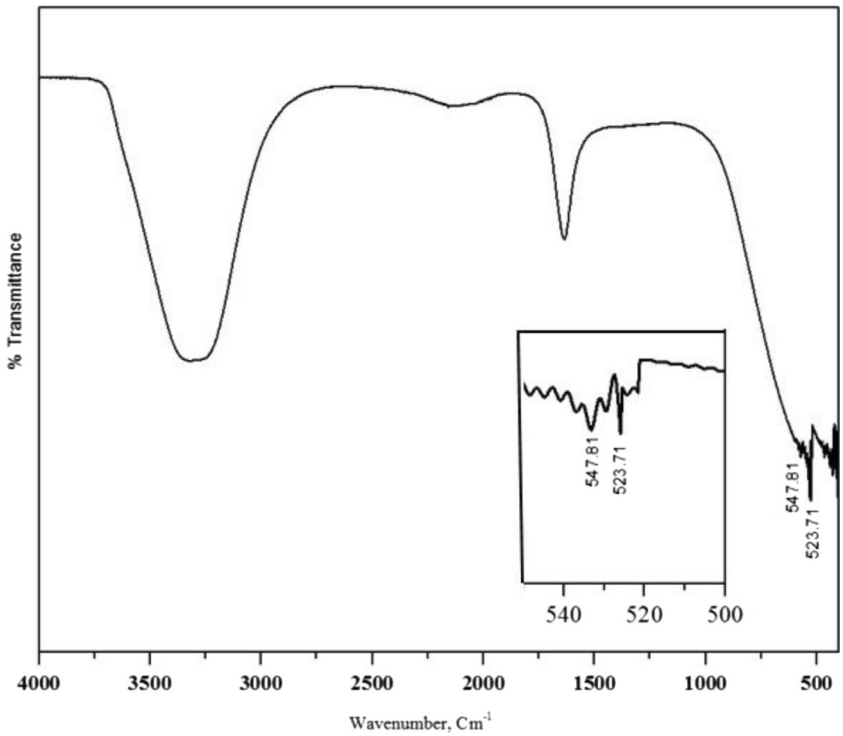

Fig. 3 FTIR spectra of α-Fe_2O_3 synthesized from neem leaves

the homogeneous solution. Finally, the solution was added dropwise to 4.0 wt% calcium chloride solutions to prepare iron oxide-impregnated calcium alginate hydrogel beads. Both the hydrogels were used for MB adsorption studies.

3 Results and Discussion

3.1 Extraction of Neem Pigment and Synthesis of Iron Oxide Nanoparticles

The amount of dry neem pigment collected from Soxhlet extraction was 11.97 g having yield of 59.85%. The % yield obtained for neem pigment was quiet high as compared to other Soxhlet extractions [18, 20].

Synthesized pigment of 5.0 g was taken in 100 mL deionized water and boiled at 80 °C for 30 min. The solution was cooled and centrifuged at 5000 rpm. The collected supernatant of 20 mL was added dropwise to 50 mL 0.1 (M) ferric chloride solution under constant stirring. The reaction temperatures were maintained at 45–50 °C, and the suspensions were stirred for 2 h. The precipitates were collected and washed several times with deionized water to get rid of any impurities. The particles were dried at 60 °C in an oven for 2 h. The schematic diagram for the preparation of neem pigment and preparation of iron oxide nanoparticles is shown in Fig. 1. The obtained iron oxide nanoparticles were characterized and used for MB degradation as well as adsorption of MB dye from aqueous solutions.

3.2 Characterization of Iron Oxide Nanoparticles

3.2.1 XRD Diffraction

The X-ray diffraction patterns of synthesized iron oxide nanoparticles are shown in Fig. 2. The nanoparticle patterns

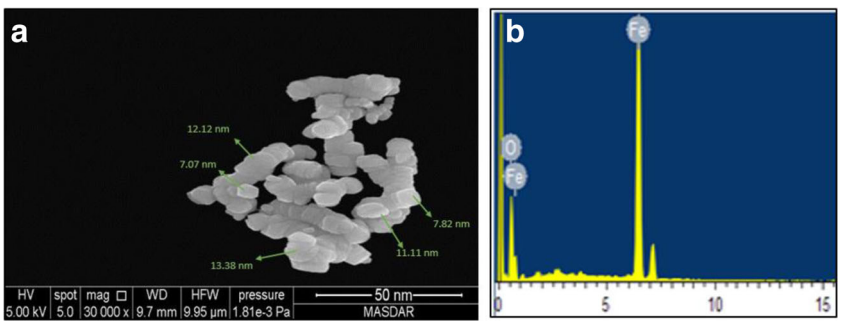

Fig. 4 (**a**) SEM and (**b**) EDX spectrum for α-Fe_2O_3 nanoparticles

Table 1 The weight and atomic weight % of different elements

Element	Weight %	Atomic weight %
O k	30.64	60.66
Fe k	69.36	39.44
Total	100	100

extracted from *A. indica* (neem) with the Bragg's law having values 24.08, 33.36, 35.59, 40.98, 45.67, 49.34, 53.95, 62.53, and 75.45° were observed. The pattern was detected at miller indices (012), (104), (110), (113), (024), (116), (122), (214), and (220) which correspond to α-Fe_2O_3 [21, 22]. The average particle size of α-Fe_2O_3 was calculated using the Debye-Scherrer equation:

$$D = k.\lambda(\beta.cos\theta) \quad (2)$$

where D is the average particle size of the particle, k is the shape factor (the typical value is 0.89), λ is the wavelength of the incident beam (0.15406 nm), θ is the Bragg diffraction angle, and β is the width of the XRD peak. The average particle size was found to be 10–20 nm [23].

3.2.2 FTIR Analysis

FTIR spectroscopy was used to identify the functional groups of the active components based on the peak value in the region of infrared radiation. Figure 3 shows FTIR spectra of iron oxide synthesized from *A. indica* (neem) extract. The formation of Fe_2O_3 is characterized by two absorption bands at 547.81 and 523.71 cm^{-1} which correspond to the Fe–O bond in hematite [24].

3.2.3 SEM and EDX Analysis

The structure and morphology of the Fe_2O_3 were studied using scanning electron microscopy and energy dispersive X-ray analysis as shown in Fig. 4. The SEM image in Fig. 4a shows the rhombohedral phase structure and is in agreement with α-Fe_2O_3 [25, 26]. In the EDX spectra (Fig. 4b), the peaks around 0.5 and 6.5 (keV) are connected to the binding energies of iron. No other peaks have been detected in the EDX, confirming that the nanoparticles are composed only with iron and oxygen.

The weight and atomic weight % of synthesized α-Fe_2O_3 are shown in Table 1.

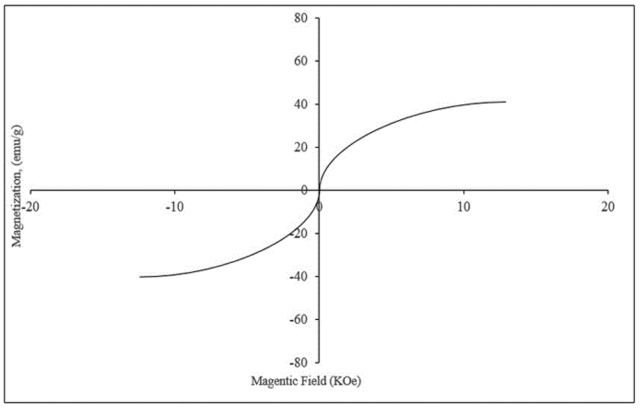

Fig. 6 Hysteresis curves of α-Fe_2O_3 nanoparticles in magnetic field

3.2.4 TEM Analysis

Transmission electron microscopy (TEM) was carried out to investigate the size and selected area electron diffraction patterns of the synthesized Fe_2O_3 particles (Fig. 5). Figure 5a illustrates that the sizes of α-Fe_2O_3 are almost uniform and all of the particles are hexagonal cone in shape with a lattice parameter (nm) a = 0.5034, c = 1.375 [26]. The observed electron diffraction pattern from Fig. 5b reveals that the synthesized α-Fe_2O_3 is single crystalline, having rhombohedral phase which was already observed in XRD studies [25].

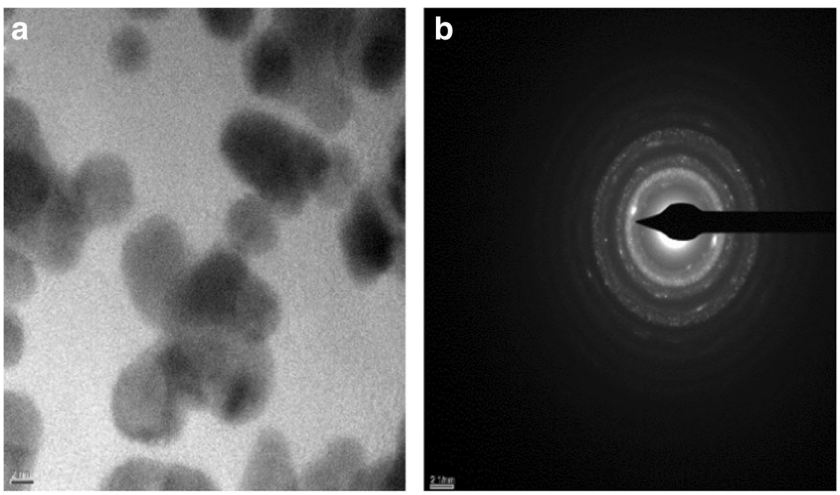

Fig. 5 (**a**) TEM and (**b**) selected area electron diffraction pattern of α-Fe_2O_3 nanoparticles

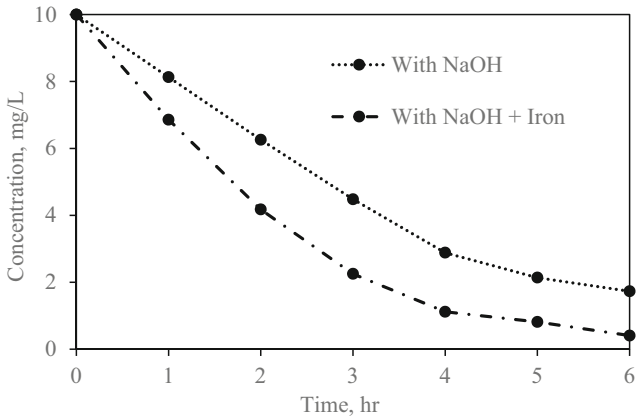

Fig. 7 Concentration of methylene blue (MB) with time

3.2.5 VSM Analysis

The magnetic properties of the iron oxide nanoparticles were characterized at room temperature using vibrating sample magnetometer [27, 28]. It was observed that pure iron oxide has 55.1 emu/g of magnetic saturation intensity at room temperature (Fig. 6). The iron oxide nanoparticles exhibit a superparamagnetic state with very low residual magnetization (8.3 emu/g) and coercive forces (91.6 Oe) at room temperature. The iron oxide nanoparticles were within 10 nm, and they might be considered to have a single magnetic domain [14].

3.3 Application

3.3.1 Catalytic Degradation of Methylene Blue (MB)

This study was performed to understand the methylene blue degradation using green-synthesized iron oxide nanoparticles in sodium hydroxide solution. The degradation was carried out in the absence of iron oxide nanoparticles also. Both the degradation kinetics are presented in this work. The degradation rate utilizing biosynthesized iron oxide nanoparticles in sodium hydroxide solution was generally controlled by the available surface area of nanoparticles [29]. Thus, a first-order degradation kinetic was applied as shown below:

$$ln\left(\frac{C}{C_0}\right) = -k_1 t \tag{3}$$

where, C_0 is initial methylene blue concentration (mg/L), C is the concentration of methylene blue at any time of degradation and k_1 is the rate constant of first-order reaction. Value of k_1 can be determined from the slope of the line by plotting $ln\left(\frac{C}{C_0}\right)$ versus time.

Consequently, the second-order kinetic model was predominantly used to describe the degradation process and was expressed in the following equation:

$$t = k_2\left(\frac{1}{C} - \frac{1}{C_0}\right) \tag{4}$$

MB is a useful molecule for free radical degradation, and its concentration dependency is monitored using UV–vis spectrophotometer (Fig. 7).

The removal of methylene blue (10 mg/L) in the presence and absence of iron oxide nanoparticles with sodium hydroxide solution was tested, and the kinetics analysis is summarized in Table 2. Values of the regression coefficients (R^2) for the first-order reduction were 0.9861 for sodium hydroxide-degraded MB and 0.9904 with iron oxide containing sodium hydroxide, respectively. It is clear that the degradation kinetics of methylene blue fitted well with first-order kinetics. This result is conclusively stated that first-order kinetic can describe the degradation process using iron oxide nanoparticles [30]. Moreover, the second-order kinetic model could not be utilized to illustrate the process for the degradation of methylene blue on the surface of iron oxide nanoparticles as all R^2 values were quiet low.

3.3.2 Adsorption of Methylene Blue (MB)

This study was performed to understand the adsorption of methylene blue dye in aqueous solutions using calcium alginate hydrogel as adsorbents and calcium alginate in the presence of green-synthesized iron oxide nanoparticles as composite hydrogel which can easily be separated from solutions using a magnet [31]. Equilibrium isotherm studies were carried out to compare the adsorption efficiency for both the adsorbents. The adsorption isotherm of MB on calcium alginate hydrogel beads in the absence and presence of iron oxide nanoparticles was generated by changing the initial concentrations of MB solutions (10–50 mg/L) with fixed amount of adsorbents (0.01 g) shaking at 120 rpm in a water bath shaker and letting the system reach equilibrium by 4.0 h. The equation used for these studies is as follows:

Table 2 Kinetics parameters for methylene blue degradation using sodium hydroxide and in the presence of α-Fe_2O_3 nanoparticles

Substrate	First-order kinetics		Second-order kinetics	
	k_1 (h^{-1})	R^2	k_2 ((mg/L) h)	R^2
Sodium hydroxide	0.2941	0.9861	0.0682	0.8983
Sodium hydroxide in the presence of α-Fe_2O_3	0.5177	0.9904	0.2673	0.7438

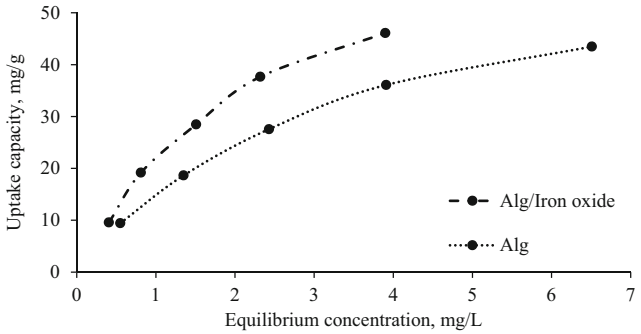

Fig. 8 Equilibrium uptake capacity versus equilibrium concentration of MB for alginate and iron oxide-impregnated alginate at room temperature

$$q_e = \left(\frac{V}{m}\right) * (C_0 - C_e) \tag{5}$$

where, q_e is the uptake capacity of adsorbents (mg/g), C_0 is initial methylene blue concentration (mg/L), C_e is the concentration of methylene blue at equilibrium, V is the volume of the MB solutions taken, and m (g) is mass of the hydrogels used. The equilibrium concentration versus uptake capacity plot is shown in Fig. 8.

The equilibrium data was fitted to Langmuir and Freundlich isotherm model to describe the best fit and was expressed as:

Langmuir model [32]:

$$q_e = \frac{q_{max} K_L C_e}{1 + K_L C_e} \tag{6}$$

where q_{max} (mg/g) is maximum adsorption capacity and K_L (L/mg) is Langmuir isotherm constant.

Freundlich model [33]:

$$q_e = K_F C_e^{1/n} \tag{7}$$

where, K_F is Freundlich constants ($mg^{1-1/n}\ L^{1/n}/g$) and n is constant of adsorption.

The adsorption of MB in the presence and absence of iron oxide nanoparticles with calcium alginate hydrogel was tested, and the equilibrium model parameters are shown in Table 3. The batch adsorption was studied using Langmuir isotherm at room temperature. A maximum uptake capacity (q_{max}) of calcium alginate for MB in the absence and presence of iron particles was found to be 64.1 and 99.0 mg/g, respectively. The Freundlich adsorption isotherm model parameters for both the adsorbents at room temperature are also shown in Table 3. The values of $\frac{1}{n}$ at each time lie in the range from 0.628 to 0.693, which supports the initial assumption of strong interactions between MB and hydrogel. The equilibrium adsorption data fitted Langmuir model better than Freundlich model as obtained from better coefficient of regression (R^2) values. Thus, the equilibrium adsorption utilizing biosynthesized iron oxide nanoparticles in calcium alginate hydrogel enhanced the adsorption process.

4 Conclusion

Neem (*A. indica*) pigment was collected efficiently using Soxhlet extraction to achieve 59.85% yield. Iron oxide (α-Fe_2O_3) nanoparticles were synthesized efficiently using extracted pigment from 0.1 (M) ferric chloride solution. Synthesized iron oxide nanoparticles were characterized using XRD, FTIR spectroscopy, SEM equipped with EDX spectroscopy, and TEM and VSM analysis. TEM analysis confirmed the presence of α-Fe_2O_3, while SEM and TEM analysis justified it to be a nanoparticle. The collected nanoparticles were evaluated for degradation and adsorption of MB dye. The degradation of MB was enhanced to 95.93% in the presence of α-Fe_2O_3 nanoparticles in 0.1 (N) sodium hydroxide solution (82.69% in the absence of nanoparticles). Similarly for the adsorption studies, the maximum uptake capacity was increased from 64.1 to 99.0 mg/g for calcium alginate hydrogel only and calcium alginate hydrogel in the presence of α-Fe_2O_3 nanoparticles (effective adsorbents as it can be easily separated using a magnet). Thus, the study illustrated the environmentally friendly practice which can be handled by biodegradable matter efficiently and bearing tremendous potential for in situ treatment process for the removal of dye molecules.

Table 3 Isotherm model parameters at room temperature

Isotherm	Parameters	Alginate	Alginate/iron oxide
Langmuir	q_{max} (mg/g)	64.1	99.0
	K_L (L/mg)	0.312	0.268
	R^2	0.999	0.994
Freundlich	K_F ($mg^{1-1/n}\ L^{1/n}/g$)	14.7	20.0
	$\frac{1}{n}$	0.628	0.693
	R^2	0.984	0.972

Acknowledgements The authors are thankful to the PIRC at the Petroleum Institute for funding this project (LTR14013) and for the SEM and VSM analysis provided by the Masdar Institute of Technology, Abu Dhabi, United Arab Emirates. Special thanks go to Anjali A. Edathil for carrying out final experimental studies.

References

1. Li, X. Q., Elliott, D. W., & Zhang, W. X. (2006). Zero-valent iron nanoparticles for abatement of environmental pollutants: materials and engineering aspects. *Sol. Sta. Mat. Sci., 31*, 111–122.
2. Kuppusamy, S., Thavamani, P., Megharaj, M., & Naidu, R. (2015). Bioremediation potential of natural polyphenol rich green wastes: a review of current research and recommendations for future directions. *Env. Tech. Inn., 4*, 17–28.
3. Ren, X., Meng, X., Chen, D., Tang, F., & Jiao, J. (2005). Using silver nanoparticle to enhance current response of biosensor. *Biosensors & Bioelectronics, 21*, 433–437.
4. Wang, C. B., & Zhang, W. X. (1997). Synthesizing nanoscale iron particles for rapid and complete dechlorination of TCE and PCBs. *Environmental Science & Technology, 31*, 2154–2156.
5. Sun, Y. G., Mayers, B., Herricks, T., & Xia, Y. N. (2003). Polyol synthesis of uniform silver nanowires: a plausible growth mechanism and the supporting evidence. *Nano Letters, 3*, 955–960.
6. Wang, T., Jin, X., Chen, Z., Megharaj, M., & Naidu, R. (2014). Green synthesis of Fe nanoparticles using eucalyptus leaf extracts for treatment of eutrophic wastewater. *Sci. Tot. Env., 466–467*, 210–213.
7. Kavitha, K. S., Syed, B., Rakshith, D., Kavitha, H. U., Rao, Y. H. C., Harini, B. P., & Satish, S. (2013). Plants as green source towards synthesis of nanoparticles. *Int. Res. J. Biological. Sci., 2*(6), 66–76.
8. Yoon, S. Y., Lee, C. G., Park, J. A., Kim, J. H., Kim, S. B., Lee, S. H., & Choi, J. W. (2014). Kinetic, equilibrium and thermodynamic studies for phosphate adsorption to magnetic iron oxide nanoparticles. *Chemical Engineering Journal, 236*, 341–347.
9. Giri, S., Samanta, S., Maji, S., Ganguli, S., & Bhaumik, S. (2005). Magnetic properties of α-Fe_2O_3 nanoparticle synthesized by a new hydrothermal method. *J. Mag. Magne. Mat., 285*, 296–302.
10. Devatha, C. P., Thalla, A. K., & Katte, S. W. (2016). Green synthesis of iron nanoparticles using different leaf extracts for treatment of domestic waste water. *Journal of Cleaner Production, 139*, 1425–1435.
11. Ahmad, A., Mukherjee, P., Mandal, D., Senapati, S., Khan, M. I., Kumar, R., & Sastry, M. J. (2002). Enzyme mediated extracellular synthesis of CdS nanoparticles by the fungus, *Fusarium oxysporum*. *Ama. Chem. Soc., 124*, 12108–12109.
12. Nadagouda, M. N., & Varma, R. S. (2008). Green synthesis of silver and palladium nanoparticles at room temperature using coffee and tea extract. *Green Chemistry, 10*, 859–862.
13. Shankar, S., Ahmad, A., & Sastry, M. (2003). Geranium leaf assisted biosynthesis of silver nanoparticles. *Biotechnology Progress, 19*(6), 1627–1631.
14. Mahdavi, M., Namvar, F., Ahmad, M. B., & Mohamad, R. (2013). Green biosynthesis and characterization of magnetic iron oxide (Fe_3O_4) nanoparticles using seaweed (*Sargassum muticum*) aqueous extract. *Mol., 18*, 5954–5964.
15. Shankar, S. S., Rai, A., Ahmad, A., & Sastry, M. (2004). Rapid synthesis of Au, Ag, and bimetallic Au core-Ag shell nanoparticles using neem (*Azadirachta indica*) leaf broth. *J. Coll. Inter. Sci., 275*(2), 496–502.
16. Patil, R. S., Kokate, M. R., & Kolekar, S. S. (2012). Bioinspired synthesis of highly stabilized silver nanoparticles using *Ocimum tenuiflorum* leaf extract and their antibacterial activity. *Spectro. Acta Part A: Mol. Biomol. Spectro., 91*, 234–238.
17. Machado, S., Pacheco, J. G., Nouws, H. P. A., Albergaria, J. T., & Matos, D. (2015). Green production of zero-valent iron nanoparticles using tree leaf extracts. *Sci. Tot. Env., 533*, 76–81.
18. Awolu, O. O., Obafaye, R. O., & Ayodele, B. S. (2013). Optimization of solvent extraction of oil from neem (*Azadirachta indica*) and its characterizations. *J. Sci. Res. Rep., 2*(1), 304–314.
19. Hossain, M. A., Al-Toubi, W. A. S., Weli, A. M., Al-Riyami, Q. A., & Al-Sabahi, J. N. (2013). Identification and characterization of chemical compounds in different crude extracts from leaves of Omani neem. *J. Tai. Uni. Sci., 7*, 181–188.
20. Banat, F., Pal, P., Jwaied, N., & Al-Rabadi, A. (2013). Extraction of olive oil from olive cake using soxhlet apparatus. *Amer. J. Oil Chem. Tech., 1*(4), 1–8.
21. Sharma, J. K., Srivastava, P., Akhtar, M. S., Singh, G., & Ameen, S. (2015). α-Fe_2O_3 hexagonal cones synthesized from the leaf extract of *Azadirachta indica* and its thermal catalytic activity. *New J. Chem., 39*, 7105–7111.
22. Zhang, X., Niu, Y., Meng, X., Li, Y., & Zhao, J. (2013). Structural evolution and characteristics of the phase transformations between α-Fe_2O_3, Fe_3O_4 and γ-Fe_2O_3 nanoparticles under reducing and oxidizing atmosphere. *Cryst. Eng. Comm., 15*, 8166–8172.
23. Cheng, Z., Tan, A. L. K., Tao, Y., Shan, D., Ting, K. E., & Yin, X. J. (2012). Synthesis and characterization of iron oxide nanoparticles and applications in the removal of heavy metals from industrial wastewater. *International Journal of Photoenergy, 2012*, 1–5.
24. Sahoo, S. K., Agarwal, K., Singh, A. K., Polke, B. G., & Raha, K. C. (2010). Characterization of γ- and α-Fe_2O_3 nano powders synthesized by emulsion precipitation-calcination route and rheological behaviour of α-Fe_2O_3. *Int. J. Eng. Sci. Tech., 2*(8), 118–126.
25. Raming, T. P., Winnubst, A. J. A., Kats, C. M. V., & Philipse, A. P. (2002). The synthesis and magnetic properties of nanosized hematite (α-Fe_2O_3) particles. *J. Coll. Inter. Sci., 249*, 346–350.
26. Teja, A. S., & Koh, P. Y. (2009). Synthesis, properties, and applications of magnetic iron oxide nanoparticles. *Prog. Cry. Gro. Char. Mat., 55*, 22–45.
27. Luo, F., Yang, D., Chen, Z., Megharaj, M., & Naidu, R. (2016). Characterization of bimetallic Fe/Pd nanoparticles by grape leaf aqueous extract and identification of active biomolecules involved in the synthesis. *J. Haz. Mat., 303*, 145–153.
28. Zhang, L., He, R., & Gu, H. C. (2006). Oleic acid coating on the monodisperse magnetite nanoparticles. *Applied Surface Science, 253*, 2611–2617.
29. Su, C., & Puls, R. W. (1999). Kinetics of trichloroethene reduction by zerovalent iron and tin: pretreatment effect, apparent activation energy, and intermediate products. *Environmental Science & Technology, 33*, 163–168.
30. Zhang, X., Lin, S., Lu, X. Q., & Chen, Z. L. (2010). Removal of Pb(II) from water using synthesized kaolin supported nanoscale zero-valent iron. *Chemical Engineering Journal, 163*, 243–248.
31. Zhang, H., Liang, X., Yang, C., Niu, C., Wang, J., & Su, X. (2016). Nano γ-Fe_2O_3/bentonite magnetic composites: synthesis, characterization and application as adsorbents. *J. Alloy. Comp., 688*, 1019–1027.
32. Langmuir, I. (1916). The adsorption of gases on plane surface of glass, mica and platinum. *J. Amer. Chem. Soc., 40*, 1361.
33. Freundlich, H. M. (1906). Over the adsorption in solution. *The Journal of Physical Chemistry, 57*, 385–470.